Spinor dynamics of quantum accelerator modes near higher-order resonances

Laura Rebuzzini,[1,2,*] Italo Guarneri,[1,2,3] and Roberto Artuso[1,3,4]

[1]*Dipartimento di Fisica e Matematica and Center for Nonlinear and Complex Systems, Università dell'Insubria, Via Valleggio 11, 22100 Como, Italy*

[2]*Istituto Nazionale di Fisica Nucleare, Sezione di Pavia, Via Ugo Bassi 6, 27100 Pavia, Italy*

[3]*CNISM, Unità di Como, Via Valleggio 11, 22100 Como, Italy*

[4]*Istituto Nazionale di Fisica Nucleare, Sezione di Milano, Via Celoria 16, 20133 Milano, Italy*

(Received 28 November 2008; published 13 March 2009)

Quantum accelerator modes were discovered in experiments with kicked cold atoms in the presence of gravity. They were shown to be tightly related to resonances of the quantum kicked rotor. In this paper a spinor formalism is developed for the analysis of modes associated with resonances of arbitrary order $q \geq 1$. Decoupling of spin variables from the orbital ones is achieved by means of an ansatz of the Born-Oppenheimer type that generates q independent band dynamics. Each of these is described, in classical terms, by a map, and the stable periodic orbits of this map give rise to quantum accelerator modes, which are potentially observable in experiments. The arithmetic organization of such periodic orbits is briefly discussed.

DOI: 10.1103/PhysRevA.79.033614 PACS number(s): 03.75.Kk, 05.45.Mt, 03.75.−b, 37.10.Vz

I. INTRODUCTION

A kicked system is a Hamiltonian system that is periodically driven by pulses of infinitesimal duration. More than 30 years after the invention of the paradigmatic model of such systems, namely the kicked rotor (KR) [1], kicked quantum dynamics is still the focus of active research for a twofold reason. On one hand, it has given birth to an ever increasing list of variants of the basic original prototypes, which have provided formally simple models for the investigation of quantum-classical correspondence and of some general properties of quantum transport. These include dynamical localization [2], anomalous diffusion [3–6], decay from stable phase-space islands [7–9], electronic conduction in mesoscopic devices [10–12], nondispersive wave-packet dynamics [13], effects of dissipation on quantum dynamics [14], and lately directed transport [15–17]. On the other hand, renewed interest on the physical side has been stimulated by experimental realizations [18–21], which are now possible, under excellent control conditions, thanks to the science and technology of cold and ultracold atoms. Unexpected advances of the theory have been prompted by such experiments. For instance, the so-called quantum accelerator modes (QAMs) were discovered in experiments with cold atoms in periodically pulsed optical lattices [22–25]. Their underlying theoretical model is a variant of the kicked rotor model, where the difference is that in between kicks, atoms are subject to gravity. When the kicking period is close to a half-integer multiple of the Talbot time [26], which is a natural time scale for the system, a fraction of atoms steadily accelerates away from the bulk of the atomic cloud at a rate and in a direction which depend on various parameter values. Though QAMs are a somewhat particular phenomenon, their theory [27–30] is a vast repertory of classic items of classical and quantum mechanics. QAMs are rooted in subtle aspects of the Bloch theory and have a relation to the Wannier-Stark resonances of solid-state physics [9]. They are a purely quantal effect, and yet they are explained in terms of trajectories of certain classical dynamical systems by means of a "pseudo-quasiclassical" approximation, where the role of the Planck constant is played by a parameter ϵ, which measures the detuning of the kicking period from a half-integer multiple of the Talbot time. This theory hinges on existence of a "pseudoclassical limit" for $\epsilon \to 0$. That means, for kicking periods close to half-integer multiples of the Talbot time, the quantum dynamics may formally be obtained from quantization of a classical dynamical system using ϵ as the Planck constant. This system is totally unrelated from the classical system that is obtained in the proper classical limit $\hbar \to 0$.

Experimental and theoretical investigations on QAMs are currently focused on novel research lines: the observation of QAMs in a Bose-Einstein condensate [31–33], which allows a precise control on the initial momentum distribution, the analysis of QAMs for special values of the physical parameters [34,35], and in particular, when the kicking period is close to a rational multiple of the Talbot time [36,37]. Theoretical aspects concerning the latter problem are considered in the present paper.

QAMs are connected with an important feature of the KR model, namely, the KR resonances [38], which occur whenever the kicking period is rationally related to the internal frequencies of the free rotor. The dynamics of the rotor at a quantum resonance (QR) is invariant under momentum translations by multiples of an integer number. The least positive integer q, such that translation invariance in momentum space holds, is of the "order" of the resonance (Sec. II). The half-Talbot time in atom-optics experiments is the period of the KR resonances of order $q=1$ (i.e., "principal" resonances), so the originally observed QAMs are related to KR resonances of order 1.

In this paper we consider quantum motion in the vicinity of a higher-order KR resonance ($q>1$) in the presence of gravity. Numerical (see Fig. 1) and heuristic indications [37] suggest that higher-order KR resonances, too, may give rise to QAMs. This has been substantiated by a theory [36] based on a nontrivial reformulation of the original pseudoclassical

*laura.rebuzzini@uninsubria.it

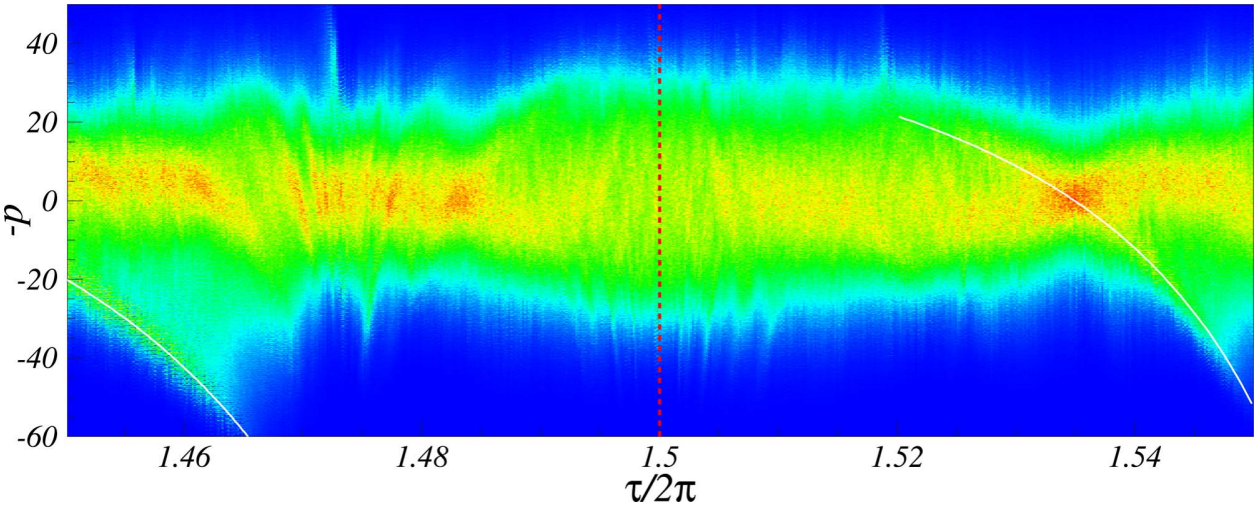

FIG. 1. (Color online) Momentum distributions in the time-dependent gauge, after $t=100$ kicks, for different values of the kicking period near the resonance $\tau_{\mathrm{res}}=3\pi$. Red color (near $p=0$) corresponds to highest probability. The vertical dashed line corresponds to the resonant value. White full lines show the theoretical curves [Eq. (32)], with (left) $q=2$, $(r,s)=(1,1)$ and (right) $q=7$, $(r,s)=(4,1)$ close to the higher-order resonance $\tau^{\mathrm{res}}/2\pi=p/q=11/7$. The initial quantum distribution is a Gaussian wave packet, reproducing the experimental conditions. The other parameters are $k=1$ and $g=0.0386$. All our numerical simulations refer to the choice $V(\theta)=k\cos\theta$. All plotted quantities are in dimensionless units.

approximation. It has been remarked that in the case of higher-order resonances, no pseudoclassical limit exists and similarity to the case of quasiclassical analysis for particles with spin was noted but not explored. About the latter general problem [39,40], it is known that although no single well-defined classical limit exists, and so no global quasiclassical phase-space approximation in terms of a unique classical Hamiltonian flow is possible, *local* quasiclassical approximations are nevertheless still possible, as provided by bundles of trajectories which belong to a number of different Hamiltonian systems.

In this paper we develop a formulation of the problem of QAMs near higher-order resonances in spinor terms. The quantum evolution at exact resonance is described by a multicomponent wave function, namely a spinor of rank q given by the order of the resonance [38,41], and is generated by a time-independent spinor Hamiltonian [42,43]. We show that the small-ϵ analysis of quantum dynamics is formally equivalent to semiclassical approximation for a particle with spin-orbit coupling. Thus QAMs near higher-order resonances constitute a particular, though experimentally relevant, model system, in which this crucial theoretical issue can be explored. The semiclassical theory in [40] is not directly applicable here because the dynamics is not specified by a self-adjoint spinor Hamiltonian but by a spinor unitary propagator instead. We therefore resort to an "adiabatic" ansatz, which allows decoupling spin dynamics from orbital motion. In this way we obtain q distinct and independent orbital one-period propagators. Each of them may be viewed as the quantization of a formally classical dynamical system, given by a map; however, the "pseudo-Planck-constant" ϵ explicitly appears in such maps in a form that precludes existence of a $\epsilon\to 0$ limit for the maps themselves, except for the $q=1$ case, in which the pseudoclassical theory of Refs. [27,28] is recovered.

QAMs, detected by numerical simulations of the exact quantum dynamics near higher-order resonances, tightly correspond to stable periodic orbits of the maps. The acceleration of the modes is expressed in terms of the winding numbers of the corresponding orbits and of the order of the resonance. Moreover, we derive some theoretical results, which generalize those obtained in [28,29] for the principal resonances: a formula for the special values of quasimomenta, which dominate the mode, and a classification of detectable modes by a Farey tree construction [44,45] as a function of the gravity acceleration.

This paper is organized as follows. In Sec. II the Floquet operator, describing the one-step evolution of a kicked atom in a free-falling frame, is recalled and the resonant spinor dynamics in kicked particle (KP) model is briefly reviewed; in Sec. III, the quantum motion in the vicinity of a resonance of arbitrary order is related to the problem of a particle with spin-orbit coupling. In Sec. IV, a "formally" classical description of the orbital dynamics, associated to the QAMs, is achieved. Finally, in Sec. V connections between the theoretical results and possible experimental findings are discussed.

II. BACKGROUND

A. Floquet operator in the temporal gauge

In the laboratory frame, the quantum dynamics of the atoms moving under the joint action of gravity and of the kicking potential is ruled by the time-dependent Hamiltonian (expressed in dimensionless units)

$$\hat{H}_L(t)=\frac{\hat{p}^2}{2}-\frac{\eta}{\tau}\hat{x}+kV(\hat{x})\sum_{n=-\infty}^{+\infty}\delta(t-n\tau), \tag{1}$$

where $\hat{p}$ and $\hat{x}$ are the momentum and position operators. The potential $V(x)$ is a smooth periodic function of spatial period

2π. By denoting M, T, K, $\mathbf{g}$, and $2\pi/G$ the atomic mass, the temporal period of the kicking, the kicking strength, the gravity acceleration, and the spatial period of the kicks, respectively, the momentum, position, and mass of the atom in Eq. (1) are rescaled in units of $\hbar G$, G^{-1}, and M; then time t and energy come in units of $M/(\hbar G^2)$ and $\hbar^2 G^2/M$. The three dimensionless parameters k, τ, and η in Eq. (1), which fully characterize the dynamics, are expressed in terms of physical quantities by $k=K/\hbar$, $\eta=M\mathbf{g}T/(\hbar G)$, and $\tau=\hbar TG^2/M=4\pi T/T_B$. $T_B=4\pi M/(\hbar G^2)$ is the Talbot time [26] and $g=\eta/\tau$ is the rescaled gravity acceleration. Throughout the following $\hbar=1$ is understood.

For $\eta=0$, Hamiltonian (1) reduces to that of the KP model, which is a well-known variant of the KR model. The KP differs from the KR because the eigenvalues of particle momentum are continuous while those of the angular momentum of the rotor are discrete. Due to Bloch theorem, the invariance of the KP Hamiltonian, under space translations by 2π, implies conservation of the quasimomentum β, which, in the chosen units, is the fractional part of the momentum. The particle momentum is decomposed as $p=N+\beta$ with $N\in\mathbb{Z}$ and $0\leq\beta<1$. Conservation of quasimomentum enables a Bloch-Wannier fibration of the particle dynamics; the particle wave function is obtained by a superposition of Bloch waves, describing the states of independently evolving kicked rotors with different values of the quasimomentum (called β rotors).

A remarkable feature of Hamiltonian (1) is that, unless rescaled gravity $g=\eta/\tau$ assumes exceptional commensurate values, the linear potential term breaks invariance under 2π space translations. Such an invariance may be recovered by going to a temporal gauge, where momentum is measured with respect to free fall. This transformation gets rid of the linear term and the new Hamiltonian reads [28]

$$\hat{H}_g(t)=\frac{1}{2}\left(\hat{N}+\beta+\frac{\eta}{\tau}t\right)^2+kV(\hat{\theta})\sum_{n=-\infty}^{+\infty}\delta(t-n\tau), \qquad (2)$$

where $\theta=x \bmod(2\pi)$, $\hat{N}=-i\partial_\theta$ with periodic boundary conditions.

The quantum motion of a β rotor in the "temporal gauge" (that is, "in the falling frame") is described by the following Floquet operator on $L^2(\mathbb{T})$ ($\mathbb{T}$ denotes the 1–torus, parametrized by $\theta\in[-\pi,\pi[$):

$$\hat{U}_\beta(n)=e^{-ikV(\hat{\theta})}\exp\{-i(\tfrac{\tau}{2})[\hat{N}+\beta+\eta n+(\tfrac{\eta}{2})]^2\}, \qquad (3)$$

where $n\in\mathbb{Z}$ denotes the number of kicks. Operator (3) describes evolution from time $t=n\tau$ to time $t=(n+1)\tau$.

B. Quantum resonances

We consider the problem of quantum accelerator modes in the vicinity of a generic resonance of the β rotor; the concept of quantum resonance is reviewed in this subsection. A QR occurs whenever quantum evolution commutes with a nontrivial group of momentum translations. A momentum translation $\hat{N}\to\hat{N}+\ell$ (recall $\hbar=1$) with $\ell\in\mathbb{Z}$ is described by the operator $\hat{T}^\ell=e^{i\ell\hat{\theta}}$. Throughout this section, we assume $\eta=0$ and then operator (3) is time independent. It commutes with $\hat{T}^\ell$ if and only if [46] (i) $\tau/2\pi=p/q$ with p and q coprime integers, (ii) $\ell=rq$ with $r\in\mathbb{N}$, and (iii) $\beta=\nu/rp+rq/2 \pmod 1$ with $\nu\in\mathbb{Z}$.

In this paper we restrict to "primary" resonances, i.e., to resonances with $r=1$ and $\ell=q$; in this case, q defines the order of the resonance. QRs of order 1 are called "principal resonances."

A theory for QAMs in the vicinity of principal resonances was proposed in [27,28]. In this paper we consider quantum resonances of arbitrary order $q\geq 1$. The resonant values of the kicking period (i), expressed in physical units, coincide with rational multiples of half of the Talbot time. We generically denote $\hat{U}_{\mathrm{res}}$ operator (3) at resonance, and β_0 the resonant values of quasimomentum, given by the above condition (iii), i.e., $\beta_0=\nu/p+q/2$ with $\nu=0,\ldots,p-1$.

C. Bloch theory and spinors

Translation invariance under $\hat{T}^q$ enforces conservation of the Bloch phase $\xi\equiv\theta \bmod(2\pi/q)$, taking values in the Brillouin zone $\mathbb{B}=[-\pi/q,\pi/q[$. Loosely speaking, this means that θ only changes by multiples of $2\pi/q$, so ξ has the meaning of "quasiposition." As we show below, at a QR, a Bloch-Wannier fibration of the rotor dynamics holds with respect to the quasiposition ξ.

We use a rescaled quasiposition $\vartheta\equiv q\xi$ and accordingly resize the Brillouin zone to $[-\pi,\pi[$. In all representations where quasiposition is diagonal, the state $|\psi\rangle$ of the rotor is described by a q-spinor ϕ, specified by q complex functions $\phi_l(\vartheta)=\langle\vartheta,l|\psi\rangle$ $(l=1,\ldots,q)$. We shall use a representation where the spinor $\boldsymbol{\phi}(\vartheta)$, which corresponds to a given rotor wave function $\psi(\theta)=\langle\theta|\psi\rangle$, is defined by

$$\phi_l(\vartheta)=\frac{1}{\sqrt{2\pi}}\sum_{m\in\mathbb{Z}}\hat{\psi}(l+mq)e^{im\vartheta}, \qquad l=0,\ldots,q-1, \qquad (4)$$

where $\hat{\psi}(n)$ $(n\in\mathbb{Z})$ are the Fourier coefficients of $\psi(\theta)$. Equation (4) defines a unitary map $\mathfrak{a}$ of $L^2(\mathbb{T})$ onto $L^2(\mathbb{T})\otimes\mathbb{C}^q$. Under this map, the (angular) momentum operator $\hat{N}$ is transformed to

$$\hat{N}=-i\partial_\theta\to\mathfrak{a}(\hat{N})\mathfrak{a}^{-1}=-iq\partial_\vartheta\otimes\hat{\mathbf{I}}+\hat{I}\otimes\hat{\mathbf{S}}, \qquad (5)$$

where $\hat{I}$ and $\hat{\mathbf{I}}$ are the identity operators in $L^2(\mathbb{T})$ and in $\mathbb{C}^q$, respectively, and $\hat{\mathbf{S}}$ is the spin operator in $\mathbb{C}^q$,

$$\hat{\mathbf{S}}=\sum_{l=0}^{q-1}l|l\rangle\langle l|, \qquad (6)$$

where $|l\rangle$, $l=0,\ldots,q-1$, is the canonical basis in $\mathbb{C}^q$. Thus, in spinor representation, the momentum operator is the sum of the orbital operator $-iq\partial_\vartheta\otimes\hat{\mathbf{I}}$ and the spin operator $\hat{I}\otimes\hat{\mathbf{S}}$. In this picture, the rotor is characterized by "orbital" observables $(\vartheta,-i\partial_\vartheta)$ and by the spin observable. Bold symbols denote vectors in $\mathbb{C}^q$ and $q\times q$ matrices.

D. Resonant spin dynamics

At resonance, quasiposition is conserved under the discrete-time evolution defined by Eq. (3), so whenever it has a definite value ϑ, no orbital motion occurs, and spin alone changes in time. Therefore the evolution is described by a unitary $q\times q$ matrix $\hat{\mathbf{A}}(\vartheta)$ such that as $\psi(\theta)$ evolves into $\hat{U}_{\rm res}\psi(\theta)$, the corresponding spinor $\boldsymbol{\phi}(\vartheta)$ evolves into the spinor $\hat{\mathbf{A}}(\vartheta)\boldsymbol{\phi}(\vartheta)$. The explicit form of the spin propagator $\hat{\mathbf{A}}(\vartheta)$ is easily computed by using Eq. (3) under resonance conditions. With the specific choice $V(\theta)=\cos(\theta)$, one finds (details can be found in Appendix A)

$$\hat{\mathbf{A}}(\vartheta) = e^{-ik\hat{\mathbf{V}}(\vartheta)}e^{-i\hat{\mathbf{G}}}, \tag{7}$$

$$\hat{\mathbf{G}} \equiv \hat{\mathbf{G}}_{p,q,\beta_0} = \pi\frac{p}{q}(\hat{\mathbf{S}} + \beta_0\hat{\mathbf{I}})^2, \tag{8}$$

$$\hat{\mathbf{V}}(\vartheta) = \frac{1}{2}\left\{\sum_{l=0}^{q-2}(|l\rangle\langle l+1| + |l+1\rangle\langle l|) + |0\rangle\langle q-1|e^{i\vartheta} + |q-1\rangle\langle 0|e^{-i\vartheta}\right\}. \tag{9}$$

Operator (7) may be written in terms of a "resonant Hamiltonian."

E. Bands

The resonant Hamiltonian $\hat{\mathbf{H}}^{\rm res}(\vartheta)$ is a Hermitian matrix of rank q such that

$$\hat{\mathbf{A}}(\vartheta) = e^{-i\hat{\mathbf{H}}^{\rm res}(\vartheta)}. \tag{10}$$

It is uniquely defined under the condition that its eigenvalues [i.e., the eigenphases of $\hat{\mathbf{A}}(\vartheta)$] lie in $[0,2\pi[$. Explicit calculation of eigenvalues and eigenvectors of $\hat{\mathbf{A}}(\vartheta)$, hence of the resonant Hamiltonian, is trivial for $q=1$ and is easily performed for $q=2$ in terms of Pauli matrices [43] (such a case is reviewed in Appendix B). However, for $q>2$ analytical calculation is prohibitive.

Eigenphases of $\hat{\mathbf{A}}(\vartheta)$ are smooth periodic function of quasiposition ϑ. As ϑ varies in $[-\pi,\pi[$, they sweep bands in the quasienergy spectrum of the resonant evolution described by $\hat{U}_{\rm res}$ [47]. They also depend on the kicking strength k and will be denoted by $\omega_l=\omega_l(\vartheta,k)$ in the following ($l=0,\ldots,q-1$). In the case $q=1$, $\omega_0(\vartheta,k)=k\cos(\vartheta)$. For $q>1$ the eigenvalues are nontrivial functions of the kick strength k. For fixed $q>2$ bandwidths tend to increase with k, eventually giving rise to complex patterns of avoided crossings. Examples of ϑ and k dependence of eigenphases are shown in Fig. 2 for (a) $q=2$ and (b) $q=7$. For $q>2$ the bandwidths depend also on l. In the resonant representation [i.e., in the representation in which the resonant propagators in Eq. (10) are diagonal], the spinor components in Eq. (4) evolve independently.

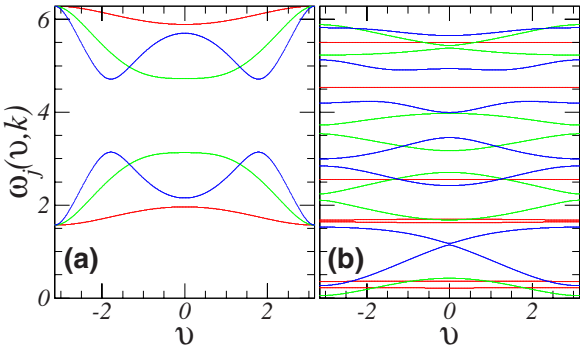

FIG. 2. (Color online) Eigenvalues of the resonant Hamiltonian $\hat{\mathbf{H}}^{\rm res}(\vartheta)$ for different values of the kicking constant $k=1$ (red), 3 (green), and 5 (blue) and (a) $q=2$, $p=3$ and (b) $q=7$, $p=11$. Wider bands in (a) correspond to higher values of k; narrower bands to small k.

III. NEAR-RESONANT DYNAMICS AND SPIN-ORBITAL DECOUPLING

We are interested in quantum motion, described by Eq. (3), in the vicinity of a QR, namely, when the kicking period is $\tau=2\pi p/q+\epsilon$, where the detuning ϵ of the period from the resonant value $\tau_{\rm res}=2\pi p/q$ is assumed to be small. The one-step evolution operator (3) may be factorized as (apart an irrelevant phase factor)

$$\hat{U}_\beta(n) = \hat{U}_{\rm res}\hat{U}_{\rm nr}(n), \tag{11}$$

$$\hat{U}_{\rm nr}(n) = \exp[-i(\tfrac{1}{2}\epsilon\hat{N}^2 + D_n\hat{N})], \tag{12}$$

where $D_n=\pi(\beta+\eta n+\eta/2)-2\pi p\beta_0/q$.

A. Adiabatic decoupling of spinor and orbital motions

Translation invariance (in momentum) is now broken by $\hat{U}_{\rm nr}$, so quasiposition is not conserved any more. The evolution of a spinor $\phi\in L^2(\mathbb{T})\otimes\mathbb{C}^q$ is ruled by the time-dependent Schrödinger equation

$$i\epsilon\frac{\partial}{\partial t}\phi = \hat{H}(t)\phi, \tag{13}$$

$$\hat{H}(t) = \epsilon\hat{H}^{\rm res}\sum_{n=-\infty}^{+\infty}\delta(t-n) + \hat{H}_0(t), \tag{14}$$

$$\hat{H}_0(t) = \frac{1}{2}\epsilon^2(-iq\partial_\vartheta\otimes\hat{\mathbf{I}} + \hat{I}\otimes\hat{\mathbf{S}})^2 + \epsilon D_{[t]}(-iq\partial_\vartheta\otimes\hat{\mathbf{I}} + \hat{I}\otimes\hat{\mathbf{S}}), \tag{15}$$

where $[t]$ denotes the integer part of t and $(\hat{H}^{\rm res}\phi)(\vartheta) = \hat{\mathbf{H}}^{\rm res}(\vartheta)\boldsymbol{\phi}(\vartheta)$. Note that $\hat{H}_0(t)$ is constant in between kicks. Both sides of the Schrödinger equation have been multiplied by ϵ to make it apparent that the detuning ϵ plays the role of an effective Planck constant in what concerns the motion between the δ-kicks.

The Hamiltonian operators $\hat{H}^{\rm res}$ and $\hat{H}_0$ are not simultaneously diagonal on the same basis. In the resonant represen-

tation, the spinor components are mixed by Eq. (15) during the evolution; we use an ansatz of the Born-Oppenheimer type in order to decouple orbital (slow) motion from spin (fast) motion.

The detuning ϵ controls as well the separation between the different time scales of the system. At exact resonance (i.e., $\epsilon=0$) the decoupling is exact because motion is restricted to the eigenspaces of the resonant propagator (10). These subspaces are defined by the spectral decomposition of the resonant Hamiltonian, which we write in the form

$$\hat{\mathbf{H}}^{\mathrm{res}}(\vartheta) = \sum_{j=0}^{q-1} \omega_j(\vartheta,k)\hat{\mathbf{P}}_j(\vartheta),$$

$$\hat{\mathbf{P}}_j(\vartheta) = |\boldsymbol{\varphi}_j(\vartheta)\rangle\langle\boldsymbol{\varphi}_j(\vartheta)|, \tag{16}$$

where $\boldsymbol{\varphi}_j(\vartheta)$ is the normalized eigenvector of $\hat{\mathbf{H}}^{\mathrm{res}}(\vartheta)$ which corresponds to the eigenvalue $\omega_j(\vartheta,k)$. For each value of ϑ, the operators $\hat{\mathbf{P}}_j(\vartheta)$ in Eq. (16) are projectors in $\mathbb{C}^q$. We denote by $\hat{P}_j$ the projectors in the full Hilbert space $L^2(\mathbb{T})\otimes\mathbb{C}^q$, which act on spinors according to $(\hat{P}_j\boldsymbol{\phi})(\vartheta)=\hat{\mathbf{P}}_j(\vartheta)\boldsymbol{\phi}(\vartheta)$. The subspaces $\mathcal{H}_j$ whereupon the $\hat{P}_j$ project are the "band subspaces" and are not invariant for the full Hamiltonian (14). By using the ansatz that band subspaces are almost invariant for small ϵ, we next decouple the (assumedly "fast") spin variables from the orbital ("slow") ones. We assume that the decoupled evolution inside the band subspaces provides a good description of the exact evolution when ϵ is small because the leading error terms are linear in ϵ.

Our approximation consists in replacing the exact dynamics, ruled by the Hamiltonian in Eqs. (14) and (15), by an adiabatic evolution generated by the Hamiltonian

$$\hat{H}^{\mathrm{diag}}(t) = \sum_{j=0}^{q-1} \hat{P}_j\hat{H}(t)\hat{P}_j = \epsilon\hat{H}^{\mathrm{res}}\sum_{n=-\infty}^{+\infty}\delta(t-n) + \sum_{j=0}^{q-1}\hat{P}_j\hat{H}_0(t)\hat{P}_j. \tag{17}$$

In the case of time-independent Hamiltonians, such projection on band subspaces, aimed at separating fast and slow time scales, is basically a Born-Oppenheimer approximation [48]. In the case of kicked dynamics this projection should be performed on the "effective," time-independent Hamiltonian $\hat{H}_{\mathrm{eff}}$, which generates over a unit time the same evolution as does the kicked Hamiltonian. The effective Hamiltonian is not known in closed form, although it can be expressed by a sum of infinite terms, ordered in powers of ϵ [43,49]. Our ansatz is somehow related to a rough approximation $\hat{H}_{\mathrm{eff}}\simeq\epsilon\hat{H}^{\mathrm{res}}+\hat{H}_0$. We assume that this is valid in some restricted parameter regimes (see further comments in Sec. IV).

A spinor in $\mathcal{H}_j$ has the form $\psi(\vartheta)\boldsymbol{\varphi}_j(\vartheta)$ with $\psi\in L^2(\mathbb{T})$ and may thus be described by a scalar wave function $\psi(\vartheta)$ (the amplitude of the spinor on the jth resonant eigenstate). Evolution inside the band subspace $\mathcal{H}_j$ is ruled by the "band Hamiltonian" $\hat{H}_j(t)=\hat{P}_j\hat{H}(t)\hat{P}_j$ and direct calculation by using Eqs. (14) and (15), shows that band Hamiltonians have the following form:

$$\hat{H}_j(t) = \epsilon\omega_j(\vartheta,k)\sum_{n=-\infty}^{+\infty}\delta(t-n) + \hat{H}_0^{(j)}(t), \tag{18}$$

where

$$\hat{H}_0^{(j)}(t) = -\frac{1}{2}\epsilon^2q^2\partial_\vartheta^2 - (\epsilon^2q^2\langle\boldsymbol{\varphi}_j|\dot{\boldsymbol{\varphi}}_j\rangle + i\epsilon^2qS_j + i\epsilon qD_{[t]})\partial_\vartheta + \frac{1}{2}\epsilon^2(S_j'' - q^2\langle\boldsymbol{\varphi}_j|\ddot{\boldsymbol{\varphi}}_j\rangle - i2qS_l') + \epsilon D_{[t]}(S_j - iq\langle\boldsymbol{\varphi}_j|\dot{\boldsymbol{\varphi}}_j\rangle). \tag{19}$$

The dots denote derivatives with respect to ϑ, and

$$S_j(\vartheta) = \langle\boldsymbol{\varphi}_j(\vartheta)|\hat{\mathbf{S}}|\boldsymbol{\varphi}_j(\vartheta)\rangle,$$

$$S_j'(\vartheta) = \langle\boldsymbol{\varphi}_j(\vartheta)|\hat{\mathbf{S}}|\dot{\boldsymbol{\varphi}}_j(\vartheta)\rangle,$$

$$S_j''(\vartheta) = \langle\boldsymbol{\varphi}_j(\vartheta)|\hat{\mathbf{S}}^2|\boldsymbol{\varphi}_j(\vartheta)\rangle. \tag{20}$$

B. Band Hamiltonians

We now note that the problem can be formulated as the evolution of a particle in a fictitious magnetic field, which takes into account the average effects of spin degree of freedom on the orbital motion. We derive a simpler form for the band Hamiltonians [Eq. (26)]. By the introduction of magnetic vector and scalar potentials, operator (19) may be written in the form

$$\hat{H}_0^{(j)}(t) = \frac{1}{2}\epsilon^2q^2[-i\partial_\vartheta - \mathcal{A}_j(\vartheta)]^2 + \epsilon qD_{[t]}[-i\partial_\vartheta - \mathcal{A}_j(\vartheta)] + \frac{1}{2}\epsilon^2\mathcal{B}_j(\vartheta). \tag{21}$$

The "geometric" vector potential $\mathcal{A}_j(\vartheta)$ and the scalar potential $\mathcal{B}_j(\vartheta)$ are determined by the structure of the resonant eigenvectors $\boldsymbol{\varphi}_j(\vartheta)$ via the following relations:

$$\mathcal{A}_j(\vartheta) = i\langle\boldsymbol{\varphi}_j(\vartheta)|\dot{\boldsymbol{\varphi}}_j(\vartheta)\rangle - \frac{1}{q}S_j(\vartheta), \tag{22}$$

$$\mathcal{B}_j(\vartheta) = S_j''(\vartheta) + 2q\mathcal{I}S_j'(\vartheta) - q^2\mathcal{A}_j^2(\vartheta) + q^2\langle\dot{\boldsymbol{\varphi}}_j(\vartheta)|\dot{\boldsymbol{\varphi}}_j(\vartheta)\rangle. \tag{23}$$

Reality of such potentials follows from Eqs. (20) and from the fact that $\langle\boldsymbol{\varphi}_j(\vartheta)|\dot{\boldsymbol{\varphi}}_j(\vartheta)\rangle$ is purely imaginary thanks to normalization. The vector potential is gauge dependent; eigenvectors $\boldsymbol{\varphi}_j(\vartheta)$ are determined up to arbitrary ϑ-dependent phase factors and so operator (21) may be further simplified by a gauge transformation, $\boldsymbol{\varphi}_j(\vartheta)\rightarrow\boldsymbol{\varphi}_j(\vartheta)e^{i\lambda_j(\vartheta)}$. Under such a transformation, $\mathcal{A}_j(\vartheta)$ changes to $\tilde{\mathcal{A}}_j(\vartheta)=\mathcal{A}_j(\vartheta)-\dot{\lambda}_j(\vartheta)$ and $\mathcal{B}_j(\vartheta)$ does not change. The transformation may be chosen so that

$$\tilde{\mathcal{A}}_j(\vartheta) = \text{const} = -\gamma_{j,q} - \varsigma \equiv \alpha_j, \tag{24}$$

where

$$\gamma_{j,q} = \frac{1}{2\pi i}\int_{-\pi}^{\pi} d\vartheta \langle \varphi_j(\vartheta) | \dot{\varphi}_j(\vartheta)\rangle,$$

$$\varsigma = \frac{1}{2\pi q}\int_{-\pi}^{\pi} d\vartheta S_j(\vartheta).$$

This immediately follows from Eq. (22) and from the requirement that eigenvectors be single valued. Note that $2\pi\gamma_{j,q}$ is the geometric (Berry's) phase [50,51]. We thus assume $\tilde{\mathcal{A}}_j = \alpha_j$; this choice corresponds to the Coulomb gauge.

In conclusion, in the jth band subspace, the band dynamics is described by the following Schrödinger equation:

$$i\epsilon\frac{\partial}{\partial t}\psi(\vartheta,t) = \hat{H}_j(t)\psi(\vartheta,t), \tag{25}$$

$$\hat{H}_j(t) = \epsilon\omega_j(\vartheta,k)\sum_{n=-\infty}^{\infty}\delta(t-n) + \frac{1}{2}\epsilon^2\mathcal{B}_j(\vartheta) + \frac{1}{2}\epsilon^2 q^2(-i\partial_\vartheta - \alpha_j)^2 + \epsilon q D_{[t]}(-i\partial_\vartheta - \alpha_j). \tag{26}$$

The multicomponent Schrödinger Eq. (13), for the q-spinor wave function $\phi(\vartheta,t)$, is then reduced to q scalar Schrödinger equations (25), each of which determines the independent evolution of a rotor wave function $\psi(\vartheta,t)$.

IV. PSEUDOCLASSICAL DESCRIPTION OF ORBITAL MOTION

We now derive a description of the dynamics of the orbital observables $(\vartheta, -i\partial_\vartheta)$, restricted inside each of the band subspaces $\mathcal{H}_j$, by formally classical equations of motion. We introduce a "pseudoclassical" momentum operator $\hat{I}$, defined as follows:

$$\hat{I} = -i\epsilon\partial_\vartheta, \tag{27}$$

which differs from the orbital momentum because of the replacement of the Planck constant (=1) by ϵ. If the same role is granted to ϵ in Eq. (25), then in classical terms, the effective band dynamics in the jth band subspace looks like a rotor dynamics, with angle coordinate ϑ and conjugate momentum I, ruled by the kicked Hamiltonian

$$H_j(\vartheta,I,t) = \epsilon\omega_j(\vartheta,k)\sum_{n=-\infty}^{+\infty}\delta(t-n) + F_j(\vartheta,I,t),$$

$$F_j(\vartheta,I,t) = \frac{1}{2}q^2I^2 + D_{[t]}qI - \epsilon q^2\alpha_j I + \frac{1}{2}\epsilon^2\mathcal{B}_j(\vartheta). \tag{28}$$

Terms, independent of I and ϑ, have been neglected. This Hamiltonian describes a classical kicked dynamics. By dropping terms beyond first order in ϵ, the map from immediately after the nth kick to immediately after the $(n+1)$th kick is

$$\vartheta_{n+1} = \vartheta_n + q^2 I_n + 2\pi\Omega qn + \varrho \mod(2\pi),$$

$$I_{n+1} = I_n - \epsilon\dot{\omega}_j(\vartheta_{n+1},k), \tag{29}$$

where $\Omega = \eta\tau/(2\pi)$ and $\varrho = q(-\epsilon q\alpha_j + \pi\Omega + \tau\beta - 2\pi p\beta_0/q)$. The meaning of the pseudoclassical map (29), as a description of the nearly resonant quantum dynamics, will be discussed in Sec. IV C.

A. Pseudoclassical maps and quantum accelerator modes

We now describe how quantum accelerator modes appear in the present framework. The explicit dependence on time of map (29) is removed by changing the momentum variable to $J_n = q^2 I_n + 2\pi\Omega qn + \varrho$. In the variables (J,ϑ) the map is 2π periodic in J and so it may be written as a map on the 2–torus,

$$\vartheta_{n+1} = \vartheta_n + J_n \mod(2\pi),$$

$$J_{n+1} = J_n - \epsilon q^2\dot{\omega}_j(\vartheta,k) + 2\pi\Omega q \mod(2\pi). \tag{30}$$

In the case of $q=1$, this map reduces to one which was introduced in [27] in order to explain the QAMs that had been experimentally observed near principal resonances. For $q>1$, it has q different versions, labeled by $j=0,\ldots,q-1$. Similar to the case $q=1$, the stable periodic orbits of each of these versions are expected to give rise to QAMs. Indeed, each stable periodic orbit of map (30) corresponds to a stable accelerating orbit of map (29) because the difference between momentum I_n and momentum J_n linearly increases with time. More precisely, let (ϑ_0, J_0) be initial conditions for a periodic orbit of period s and winding number r/s. The increment of J after time ns (measured in the number of kicks) is $2\pi rn$; therefore, the increment of the original momentum variable is

$$I_{sn} - I_0 = a_I sn, \quad a_I = \frac{2\pi}{q}\left(\frac{r}{qs} - \Omega\right), \tag{31}$$

with $I_0 = (J_0 - \varrho)/q^2$. This formula (31) yields the acceleration of a stable orbit of the pseudoclassical dynamics (29), and it is precisely this orbit that may give rise to QAMs in the vicinity of resonances of arbitrary order. As a matter of fact, numerical simulations reveal QAMs near higher-order resonances, in correspondence with periodic orbits of maps in Eq. (30). In Sec. V, we explain how the analysis of the stable periodic orbits of maps in Eq. (30) may help to resolve the complex pattern of QAMs presented in Fig. 1.

Thanks to Eqs. (5) and (27), the physical momentum N is related to I by $N = qI/\epsilon + j$; therefore, the physical acceleration is given by

$$a = \frac{2\pi}{\epsilon}\left(\frac{r}{qs} - \Omega\right). \tag{32}$$

Although the analytical derivation of the maps is based on the resonant Hamiltonian, which is known in closed form only for $q=1,2$, the practical use of Eqs. (30) only requires the resonant eigenvalues, which can be easily computed by a numerical diagonalization of a $q\times q$ matrix.

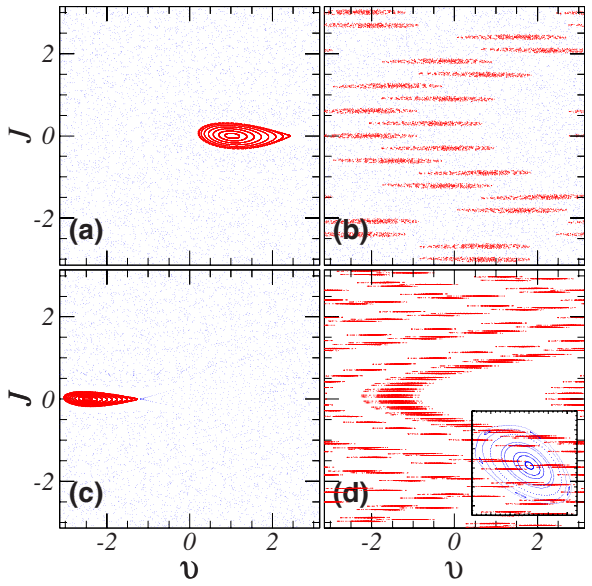

FIG. 3. (Color online) Phase portraits of the two-torus maps with $k=1$ ($\tilde{k}=\epsilon$) and $g=0.0386$. (a) and (b) refer to map (37) with $m_{p,\nu}=1$; (c) and (d) refer to Eq. (30). The periodic orbit in (d) has period $s=132$ and is associated to 132 stability islands; r and s are not coprime ($r=1056$, $s=132$). One of the small islands of the chain is magnified in the inset. The values of p/q; $\tau/2\pi$; (ϵ); $2\pi\Omega$; (r,s); and j are respectively: (a) 3/2, 1.445 (-0.2827), 3.2261, (1,1), 1; (b) 3/2, 1.5025 (0.0157), 3.4401, (23,21), 0; (c) 11/7, 1.5375 (0.2132), 3.6023, (4,1), 3; (d) 22/15, 1.485 (0.1152), 3.3605, (8,1), 15.

In Fig. 3, examples of phase space of maps in Eq. (30) are shown for (a) and (b) $q=2$, (c) $q=7$, and (d) $q=15$, in parameter regimes in which QAMs are present. The plotted periodic orbits correspond to some of the modes shown in Fig. 1. For instance, in Fig. 3(a) the stability island of a fixed point of one of the maps in Eq. (37) for $q=2$ is plotted for $\tau/2\pi=1.455$; this fixed point corresponds to the huge mode on the left side of Fig. 1. As shown in Fig. 4, a distribution of phase-space points, which initially fall inside the stability island, describes an ensemble of atoms generating the QAM.

Of the q maps in Eqs. (30), the one, which crucially contributes in determining the observed QAMs, is generally that with the widest bandwidth; indeed this map presents, in most cases, classical structures, such as stability islands, with an area greater than the effective Planck constant ϵ and thus supporting many quantum states [9]. However, also islands with a size comparable or smaller than ϵ, and scars, related to unstable periodic orbits, may affect the quantum system, giving rise to minor structures in the atomic momentum distribution [28].

B. Special values of quasimomenta

A QAM arises when the initial wave packet is centered in momentum N_0, related to I_0 by

$$N_0 = q\frac{I_0}{\epsilon} + j = \frac{1}{q\epsilon}(J_0 + 2\pi n) + q\alpha_j - \frac{1}{\epsilon}(\pi\Omega + \tau\beta - 2\pi p\beta_0/q) + j, \tag{33}$$

with $n \in \mathbb{Z}$. As in the case for main resonances, we expect

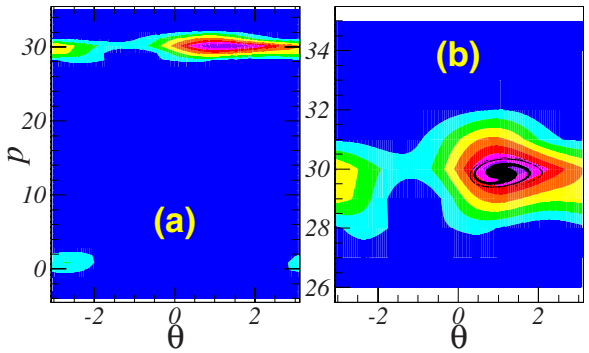

FIG. 4. (Color online) (a) Contour plot at time $t=100$ of the Husimi distribution of the wave packet of a β rotor with $\beta=0.1672$, given by Eq. (39) with $N_0=J_0=0$, $p=3$, $\nu=0$, and $n=1$. The rotor is initially prepared in a coherent state centered in the $(r,s)=(1,1)$ fixed point of Fig. 3(a). (b) Magnification of (a). The black spots in the centers of the contours are an ensemble of classical phase points, initially distributed in a circle of area $\sim\epsilon$ centered at the mode. They evolve according to the ϵ-classical dynamics (38) with $\varrho=-0.5709$. The other parameter values are $k=1$, $\tau=1.455\times 2\pi(\epsilon=-0.2827)$, and $g=0.0386$.

that the modes will be especially pronounced when quasimomentum is fine tuned; in view of Eq. (33) such optimal values of β are determined by the condition

$$\beta_\nu = -\frac{\epsilon}{\tau}(N_0 - j - q\alpha_j + \beta_0) - \frac{J_0 + 2\pi m}{q\tau} + -\frac{\eta}{2} + \beta_0 \mod(1), \tag{34}$$

with $\beta_0=\frac{\nu}{p}+\frac{q}{2}$ and $\nu=0,1,\ldots,p-1$. A wave packet initially localized in $N_0+\beta_\nu$ will be mostly captured inside a QAM; indeed in this case, the overlap between the stability island and the initial wave packet is maximal. Formula (34) is a generalization of the result derived for $q=1$ in [27] and experimentally verified in [31]; it reduces to the expression in [27] for $\alpha_0=0$ [see Appendix B].

This picture is confirmed by Fig. 4, in which the quantum phase-space evolution of a β rotor, with a quasimomentum given by Eq. (34), and the pseudoclassical motion are compared. The initial state of the rotor is a coherent wave packet centered in the $(r,s)=(1,1)$ fixed point, plotted in Fig. 3(a), corresponding to the ϵ-classical accelerator mode on the left part of Fig. 1, in the vicinity of $q=2$ resonance. The mode moves with an acceleration equal to 0.2988 according to Eq. (32).

C. Validity of the pseudoclassical description

We now come back to the meaning of the pseudoclassical description, as pseudoclassical dynamics (29) still explicitly retains the "Planck constant" ϵ. In the case when $q=1$, there is a single resonant eigenvalue, given by $\omega_0(\vartheta,k)=k\cos(\vartheta)$, so the pseudoclassical dynamics (29) has a well-defined limit for $\epsilon\to 0$, $k\to\infty$, and $k\epsilon\to\tilde{k}$ with $|\tilde{k}|<\infty$. This limit dynamics was discovered and analyzed in [27,28]. This is no longer true when $q>1$, and then the relation between the band dy-

namics and the pseudoclassical dynamics (29) is less transparent. The quantum band dynamics is still, formally, the quantization of the classical kicked dynamics (29) using ϵ as the Planck constant. Nevertheless, the latter dynamics contains the Planck constant ϵ in crucial ways, which preclude existence of a limit for $\epsilon \to 0$. To see this, note that $\omega_j(\vartheta,k)$ depends on its arguments only through the real variables $u = k \sin(\vartheta/q)$ and $v = k \cos(\vartheta/q)$ [cf. the form of the resonant evolution (A3) in Appendix A], that is, $\omega_j(\vartheta,k) = G(u,v)$, where G is a smooth oscillatory function independent of k. Hence,

$$\epsilon\dot{\omega}_j(\vartheta,k) = \frac{\epsilon k}{q}\{\cos(\vartheta/q)\partial_u G - \sin(\vartheta/q)\partial_v G\}. \quad (35)$$

Existence of a limit demands $\epsilon k \to \tilde{k}$; but then, except in the trivial case $\tilde{k}=0$, the arguments of the G functions in Eq. (35) diverge and so the second term of Eq. (35) appears to oscillate faster and faster as $\epsilon \to 0$ without a well-defined limit.

Nonexistence of a pseudoclassical limit for the quantum dynamics was established in [36], by a stationary phase approach, with no recourse to the band formalism. It was nonetheless pointed out that despite absence of such a limit, QAMs may be associated to certain rays, which correspond to trajectories of some formally classical maps. The meaning of the latter maps is, at most, that of providing local phase-space descriptions near QAMs. Similar remarks apply in the case of the pseudoclassical maps in Eq. (29).

It is worth recalling that maps in Eq. (29) were derived from an ansatz, which would be optimally justified if the effective Hamiltonian of kicked dynamics could be replaced by the sum of the free and of the kicking Hamiltonians (Sec. III). This approximation is obviously invalid in a global sense, yet in spinless cases, it is known to work remarkably well near stable fixed points [9]; indeed, in the KR case it yields a pendulum Hamiltonian, which provides a good description of the motion near the stable fixed point of the standard map. This may be seen as a qualitative justification for the use of maps in Eq. (29) if restricted to the search of QAMs.

D. Case $q=2$

While the expressions in Sec. IV A are quite general, we may accomplish a detailed analysis when $q=2$ and $V(\theta) = k\cos(\theta)$. We recall that the resonant values of quasimomenta are $\beta_0 = \nu/p$ with $\nu = 0,\ldots,p-1$ according to (iii) in Sec. II B.

In such a case the eigenvalues $\omega_j(\vartheta,k)$ $(j=0,1)$ of the resonant Hamiltonian can be written down explicitly (see Appendix B),

$$\omega_j = \frac{\pi}{2}\frac{\nu^2}{p} - m_{p,\nu}\left[\frac{\pi}{4} + (-1)^j \arccos\left(\frac{\cos v}{\sqrt{2}}\right)\right], \quad (36)$$

with $v = k\cos(\vartheta/2)$ and $m_{p,\nu} = (-1)^{[(p+1)/2]+\nu}$.

Therefore, our theory produces two maps [Eqs. (30)], which take the form

$$\vartheta_{t+1} = \vartheta_t + J_t \mod(2\pi),$$

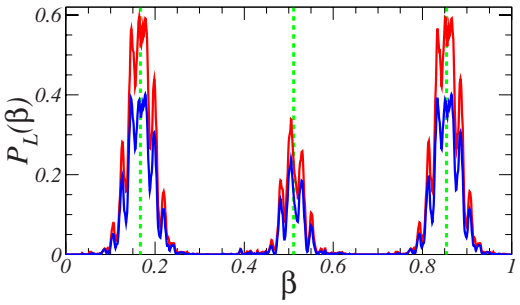

FIG. 5. (Color online) Probability inside a box of extension equal to $L=6\simeq \Delta J q/|\epsilon|$ in momentum, moving according to Eq. (32) for $p=3$, $q=2$, $(r,s)=(1,1)$, and $\epsilon=-0.2828$ as a function of quasimomentum β of the β rotor. ΔJ is the size of the island in J, plotted in Fig. 3(a). Dashed vertical lines refer to special values of quasimomenta, given by formula (39) with $\nu=0,1,2$ and $N_0=J_0=0$, $n=1$, and $\eta=g\tau=0.3529$. The probability is shown at time $t=100$ (red, or higher curve) and $t=200$ (blue curve). The parameter values are the same as in Fig. 1.

$$J_{t+1} = J_t + 4\pi\Omega + 2\tilde{k}h_j(\vartheta_{t+1}) \mod(2\pi), \quad (37)$$

with

$$h_j(\vartheta) = -m_{p,\nu}(-1)^j \sin\left(\frac{\vartheta}{2}\right)\frac{\sin[k\cos(\frac{\vartheta}{2})]}{\sqrt{1+\sin^2[k\cos(\frac{\vartheta}{2})]}}.$$

Going back to the time-dependent form, the maps are written as

$$\vartheta_{t+1} = \vartheta_t + 4I_t + 4\pi\Omega t + \varrho \mod(2\pi),$$

$$I_{t+1} = I_t + \frac{\tilde{k}}{2}h_j(\vartheta_{t+1}), \quad (38)$$

with $\varrho = 2(\epsilon\delta_{j,1} + \pi\Omega + \tau\beta - \pi\nu)$ and where we have used $\alpha_j = -\frac{1}{2}\delta_{j,1}$ [see Appendix B].

We remark that in the case $q=2$, there aren't any avoided crossings between the eigenvalues [Eq. (36)], for an arbitrary value of k. We may also check the selection criterion for quasimomenta that in the present case assumes the form

$$\beta_\nu = -\frac{\epsilon}{\tau}\left(N_0 + \frac{\nu}{p}\right) + \frac{J_0 + 2\pi n}{q\tau} - \frac{\eta}{2} + \frac{\nu}{p} \mod(1), \quad (39)$$

with $\nu = 0,\ldots,p-1$. A scan over possible β values reveals that indeed QAMs are greatly enhanced around the values predicted by Eq. (39); this is confirmed by Fig. 5, in which the momentum probability transferred to the mode is shown as a function of β.

V. MODE SPECTROSCOPY AND CONNECTIONS WITH COLD ATOM EXPERIMENTS

A. Farey ordering of QAMs near a fixed resonance

We now elucidate how our findings apply to inspection of density plots similar to the one illustrated in Fig. 1. We point out that such a picture is of direct physical significance since typical experimental protocols maintain k and g fixed while

performing a scan on the pulse period τ. Such a scan, in the present context, has to be carried out around a resonant value, namely, $\tau(\epsilon)=2\pi p/q+\epsilon$. Density plots of momentum distribution disclose the presence of QAMs, since after a fixed number of kicks their momentum is linearly related to acceleration (32); a depends on ϵ through the "bare" winding number $q\Omega$,

$$q\Omega(\epsilon)=\frac{q}{2\pi}g\left(2\pi\frac{p}{q}+\epsilon\right)^2, \tag{40}$$

and on the "dressed" winding number of the pseudoclassical map r/s, which individuates the mode. We denote by Ω^* the resonant ($\epsilon=0$) value of the bare winding number (notice that for $\epsilon=0$ the maps correspond to pure rotation in J),

$$\Omega^* \equiv q\Omega(0)=2\pi\frac{p^2}{q}g, \tag{41}$$

which is independent of the mapping index j. Formula (41) is a generalization of the analogous result found for $q=1$ [29,52].

As analyzed in [29,52] for principal resonances, the parameter space of map (30) is characterized by the presence of regions (Arnold tongues), in which stable periodic orbits exist. Close to resonances we expect that mode-locking structure of the pseudoclassical maps singles out modes whose winding number provides rational approximants to Ω^*; at the same time fat tongues are associated to small s values so the corresponding modes should be more clearly detectable. This is the physical motivation underlying Farey organization of observed modes; whenever we observe two modes labeled by winding numbers r_1/s_1 and r_2/s_2 ($r_1/s_1<\Omega^*<r_2/s_2$), the fraction with the smallest denominator bracketed by the winding pair is the Farey mediant $(r_1+r_2)/(s_1+s_2)$.

We can now analyze in more detail (Fig. 1) which represents a numerical simulation of experimental momentum distribution after $t=100$ vs τ, which assumes values around a second-order resonance, namely, $\tau^{\rm res}/2\pi=p/q=3/2$. All parameters are chosen to be accessible to experiments and the initial atomic distribution reproduces that employed in [22–25]; $g=0.0386$, $k=1$, and the initial state is a mixture of 100 plane waves sampled from a Gaussian distribution of momenta with full width at half maximum (FWHM) ~ 9. Full lines in the figure delineate momentum profiles consistent with acceleration (32), with (r,s) given by winding number r/s of corresponding stable periodic orbits of maps [Eq. (30)].

The value of Ω^* and the first few rational approximants (obtained upon successive truncation of the continued fraction expansion), corresponding to detectable modes, are

$$\Omega^* \simeq 1.091\ 389\ 3=1+[10,1,16,3,3,\ldots],$$

$$\frac{r}{s}=1,\quad \frac{11}{10},\quad \frac{12}{11},\ldots \tag{42}$$

The first one $(r,s)=(1,1)$ is shown with the white line on the left of Fig. 1 and the stability island of the corresponding fixed point is shown in Fig. 3(a). The second and third are marked by full yellow lines in Fig. 6, which is an enlargement of Fig. 1 in the region $1.49\leq\tau/2\pi\leq 1.506\ 25$, calculated for time $t=200$. Farey organization is exemplified by the appearance of the (23, 21) QAM, whose winding number is the Farey composition of the (11, 10) and the (12, 11) modes; the correspondent stable periodic orbit is plotted in Fig. 3(b). Through Farey composition law we may also identify observed modes to the left of $\tau_{\rm res}$, as shown in Fig. 6.

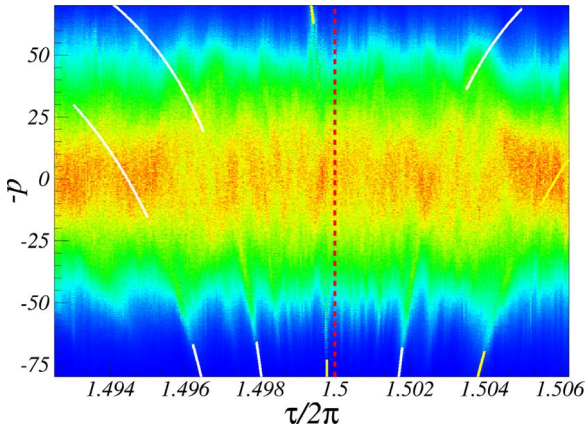

FIG. 6. (Color online) Enlargement of Fig. 1 in the region $1.49\leq\tau/2\pi\leq 1.506\ 25$ around the resonance $\tau_{\rm res}=3\pi$ ($p/q=3/2$). Momentum distributions are calculated after $t=200$ kicks. Full lines show the theoretical curves [Eq. (32)]; the yellow ones refer to principal convergents of Ω^*, listed in Eq. (42). Starting from the left, the modes correspond to the stable periodic orbits of maps in Eq. (37) with $(r,s)=(14,13)$, (25, 23), (12, 11), (23, 21), and (11, 10).

B. Visibility of resonances of different order

The complexity of mode spectroscopy is further enhanced by the fact that within some interval in τ, arbitrarily many different resonant values occur. As a matter of fact it is possible to recognize in Fig. 1 the modes coming from a wide set of resonances; besides $q=2$ also $q=7,15,17,21,36,40$ contribute QAMs in the selected range; this is shown in Fig. 1 for $q=7$ and in Fig. 7 for the other resonances. No QAM with $q=13$ could be resolved in the range of Fig. 1.

Farey composition is still of some use in the identification of the resonances to which modes they belong; for instance, the very large mode on the right of the figure belongs to a QR between $p/q=3/2$ and $p/q=2/1$; applying Farey composition successively, we get the sequence $p/q=5/3,8/5$ (outside the plotted range in τ) and then 11/7, to which the mode belongs to. The accumulation point of the resonance $p/q=11/7$ is $\Omega^*\simeq 4.192\ 320\ 7=4+[5,\ldots]$. The mode shown in Fig. 1 corresponds to the first principal convergent of Ω^*, i.e., to the fixed point $(r,s)=(4,1)$, shown in Fig. 3(c). The same occurs for the modes near resonances of higher q, shown in Fig. 7.

We remark that a hierarchy in resonant fractions looks more cumbersome than the one considered for winding numbers, as for instance there does not seem to be any straightforward dependence on the size of q. Numerical data however suggest that detectable modes appear in the vicinity of resonances leading to almost integer Ω^*, i.e., when the frac-

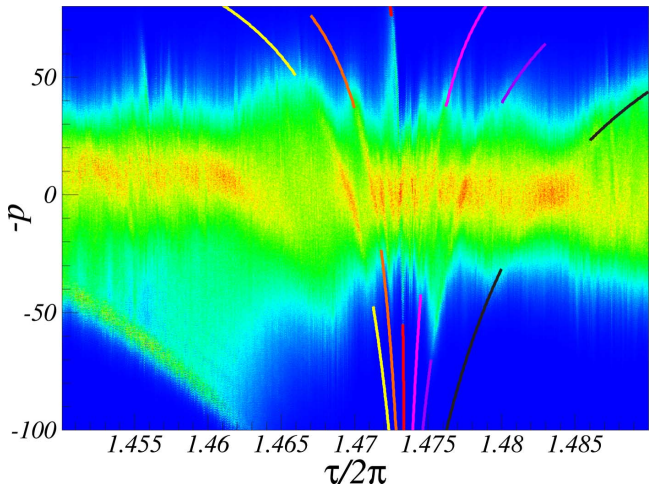

FIG. 7. (Color online) Enlargement of Fig. 1 in the region $1.45 \leq \tau/2\pi \leq 1.49$. The momentum distributions are calculated after $t=200$ kicks. Full lines show the theoretical curves in Eq. (32); each color refers to a different quantum resonance, namely, different values of p/q. Starting from the left the modes correspond to $p/q=3/2$ (theoretical curve not shown), 31/21, 59/40, 28/19, 53/36, 25/17, and 22/15. These resonances p_n/q_n lead to almost integer Ω^* and they are selected from the sequence of Farey fractions obtained starting from $p_0/q_0=1/1$ and $p_1/q_1=3/2$; starting from the right of the figure, the following resonances p/q can be found $p_8/q_8=22/15$, $\Omega_8^* \simeq 7.825\,66=8-[5,\ldots]$, and $(r,s)=(8,1)$ (shown in black); $p_9/q_9=25/17$, $\Omega_9^* \simeq 8.916\,579\,1=9-[11,\ldots]$, and $(r,s)=(9,1)$ (in purple); $p_{10}/q_{10}=28/19$; $\Omega_{10}^* \simeq 10.0075=10+[131,\ldots]$, and $(r,s)=(10,1)$ (in red); $p_{11}/q_{11}=31/21$, $\Omega_{11}^* \simeq 11.098\,678=11+[10,\ldots]$, and $(r,s)=(11,1)$ (in yellow). Further modes are shown in between the mentioned ones, $p/q=53/36=25/17 \oplus 28/19$ with $\Omega^* \simeq 18.924\,152=19-[13,\ldots]$ (shown in pink) and $p/q=59/40=28/19 \oplus 31/21$ with $\Omega^* \simeq 21.106\,256=21+[9,\ldots]$ (shown in orange). The (8,1)-periodic orbit of the resonance $p_8/q_8=22/15$ is plotted in Fig. 3(d).

tional part of Ω^* is closer to the integers 0 or 1 than to their Farey mediant 1/2. In these cases, the resonance may display a mode corresponding to a periodic orbit of period 1. As shown in Fig. 7, this condition may be fulfilled for different p/q values. Moreover, the absence of observable QAMs with $q=13$ in the range of Fig. 1, even if $p/q=20/13$ resonance belongs to the plotted τ range, is consistent with this rough "thumb" rule. Indeed $\Omega^* \simeq 7.462\,490\,8=7+[2,6,6,\ldots]$, thus its fractional part is closer to 1/2 than to 0.

VI. CONCLUSIONS AND OUTLOOK

The quantum dynamics of quantum accelerator modes, experimentally observed by exposing cold atoms to periodic kicks in the direction of the gravitational field, is theoretically described in terms of spinors when the pulse period is close to a rational multiple of a characteristic time of the atoms (Talbot time). The reference model is a nontrivial variant of the well-known kicked rotator in an almost-resonant regime. If the detuning of the kicking period to the resonant value is assigned the role of the Planck constant, the problem is shown to share similarities with the semiclassical limit of the particle dynamics in presence of spin-orbital coupling. The separation of the spinor and orbital degrees of freedom is based on an adiabatic assumption of Born-Oppenheimer type, valid for small detunings and for values of the parameters in which the QAMs manifest. In these parameter regimes, a description of some properties of the slow orbital motion, by means of formally classical equations, is achieved. Some results of a previously formulated pseudoclassical theory [28], restricted to QAMs near principal resonances, are extended to arbitrary higher-order resonances. Potential applications to current experiments on cold atomic gases are proposed.

The theoretical treatment of higher-order QAMs, presented in this paper, relies on the concept of quantum resonance of the system at zero gravity. An alternative theoretical approach may be obtained starting from a more general definition of quantum resonance, including the contribution of gravity acceleration, as done in [34,53] for principal resonances. This approach, which is applicable for values of gravity in the vicinity of the resonant ones, may allow one to refine the range of validity of the physical parameters of the spinor description.

ACKNOWLEDGMENT

L.R. acknowledges useful discussions with Shmuel Fishman.

APPENDIX A: SPINOR DYNAMICS AT EXACT RESONANCE AND WITHOUT GRAVITY

The Floquet operator at exact resonance in absence of gravity $\eta=0$ is given by [cf. Eq. (3)]

$$\hat{U}_{\rm res} = e^{-ikV(\hat{\theta})} \exp[-i\pi\tfrac{p}{q}(\hat{N}+\beta_0)^2]. \tag{A1}$$

where $\beta_0=\nu/rp+rq/2$ with $\nu \in \mathbb{Z}$. The evolution of spinor components $\phi_j(\vartheta)$ under $\hat{U}_{\rm res}$ is given by [47]

$$\bar{\phi}_j(\vartheta) = \sum_{l=0}^{q-1} (e^{-ik\hat{V}})_{j-l} \exp[-i\pi\tfrac{p}{q}(l+\beta_0)^2]\phi_l(\vartheta), \tag{A2}$$

$$\begin{aligned}(e^{-ik\hat{V}})_{j-l} &= \langle j|\exp[-i\tfrac{\vartheta}{q}\hat{\mathbf{S}}]\hat{\mathbf{F}}e^{-ik\hat{V}(\theta)}\hat{\mathbf{F}}^\dagger \exp[i\tfrac{\vartheta}{q}\hat{\mathbf{S}}]|l\rangle \\ &= \frac{\exp[-i(j-l)\frac{\vartheta}{q}]}{q}\sum_{m=0}^{q-1}\exp[-i\tfrac{2\pi}{q}m(j-l)] \\ &\quad \times \exp[-ik\hat{V}(\tfrac{\vartheta}{q}+\tfrac{2\pi}{q}m)].\end{aligned} \tag{A3}$$

$\hat{\mathbf{F}}$ is the Fourier transform in $\mathbb{C}^q$, $\langle j|\hat{\mathbf{F}}|l\rangle = \exp[-i\frac{2\pi}{q}jl]/\sqrt{q}$, and $\hat{\mathbf{S}}$ is the spin operator (6). Hence from Eq. (A2), the resonant Floquet operator is decomposable in spin propagators $\hat{\mathbf{A}}(\vartheta)$, given by unitary matrices of rank q; namely, it acts as $(\hat{U}_{\rm res}\phi)(\vartheta)=\hat{\mathbf{A}}(\vartheta)\phi(\vartheta)$.

APPENDIX B: CASE $q=2$—RESONANT EIGENVALUES AND EIGENVECTORS

At primary second-order ($q=2$) resonances, the resonant values of quasimomentum are $\beta_0=\nu/p$ with $\nu=0,1,\ldots,p-1$. We choose $V(\theta)=k\cos(\theta)$. From Eqs. (8) and (9), denoting $v(\vartheta,k)=k\cos(\vartheta/2)$, we find

$$\hat{\mathbf{A}} = \exp\left(-i\frac{\pi}{2}\frac{\nu^2}{p}\right) \times \begin{pmatrix} \cos v(\vartheta,k) & m_{p,\nu}\exp\left(i\frac{\vartheta}{2}\right)\sin v(\vartheta,k) \\ -i\exp\left(-i\frac{\vartheta}{2}\right)\sin v(\vartheta,k) & i m_{p,\nu}\cos v(\vartheta,k) \end{pmatrix}, \tag{B1}$$

with $m_{p,\nu}=(-1)^{[(p+1)/2]+\nu}$.

Matrix (B1) can be written in terms of Pauli matrices $\vec{\boldsymbol{\sigma}}$ as follows:

$$\begin{aligned}\hat{\mathbf{A}} &= \exp\left(-i\frac{\pi}{2}\frac{\nu^2}{p}\right)\exp\left(i m_{p,\nu}\frac{\pi}{4}\right)[\cos\bar{\omega}(\vartheta,k) + i\vec{x}(\vartheta,k)\cdot\vec{\boldsymbol{\sigma}}] \\ &= \exp\left(-i\frac{\pi}{2}\frac{\nu^2}{p}\right)\exp\left(i m_{p,\nu}\frac{\pi}{4}\right)[\cos\bar{\omega}(\vartheta,k) \\ &\quad + i\sin\bar{\omega}(\vartheta,k)\vec{\boldsymbol{n}}(\vartheta,k)\cdot\vec{\boldsymbol{\sigma}}],\end{aligned} \tag{B2}$$

where

$$\bar{\omega}(\vartheta,k) = \arccos\left(\frac{\cos[k\cos(\vartheta/2)]}{\sqrt{2}}\right)$$

and the vector $\boldsymbol{x}(\vartheta,k)\in\mathbb{R}^3$ has the components

$$\begin{aligned} x_1(\vartheta,k) &= m_{p,\nu}\sin\left(\frac{\vartheta}{2} - m_{p,\nu}\frac{\pi}{4}\right)\sin v(\vartheta,k), \\ x_2(\vartheta,k) &= \sin\left(\frac{\vartheta}{2} + m_{p,\nu}\frac{\pi}{4}\right)\sin v(\vartheta,k), \\ x_3(\vartheta,k) &= -\frac{m_{p,\nu}}{\sqrt{2}}\cos v(\vartheta,k). \end{aligned} \tag{B3}$$

$\vec{\boldsymbol{n}}=\vec{\boldsymbol{x}}/x$ is a unit vector in $\mathbb{R}^3$ and $x(\vartheta,k)=\|\boldsymbol{x}(\vartheta,k)\|$.

Using a well-known formula, Eq. (B2) may be written as

$$\hat{\mathbf{A}} = \exp\left(-i\frac{\pi}{2}\frac{\nu^2}{p}\right)\exp\left(i m_{p,\nu}\frac{\pi}{4}\right)e^{i\bar{\omega}(\vartheta,k)\vec{\boldsymbol{n}}(\vartheta,k)\cdot\vec{\boldsymbol{\sigma}}}, \tag{B4}$$

which directly yields to the resonant Hamiltonian for this case,

$$\hat{\mathbf{H}}^{\mathrm{res}} = \frac{\pi}{2}\frac{\nu^2}{p} - m_{p,\nu}\frac{\pi}{4} - \bar{\omega}(\vartheta,k)\vec{\boldsymbol{n}}(\vartheta,k)\cdot\vec{\boldsymbol{\sigma}}. \tag{B5}$$

As the matrix $\vec{\boldsymbol{n}}\cdot\vec{\boldsymbol{\sigma}}$ has eigenvalues ±1, the eigenvalues of the resonant fiber (B4) are

$$\begin{aligned}\lambda^{(j)}(\vartheta,k) &= \exp\left(-i\left\{\frac{\pi}{2}\frac{\nu^2}{p} - m_{p,\nu}\left[\frac{\pi}{4} + (-1)^j\bar{\omega}(\vartheta,k)\right]\right\}\right) = e^{-i\omega_j(\vartheta,k)}, \\ \omega_j(\vartheta,k) &= \frac{\pi}{2}\frac{\nu^2}{p} - m_{p,\nu}\left[\frac{\pi}{4} + (-1)^j\bar{\omega}(\vartheta,k)\right], \quad j=0,1.\end{aligned} \tag{B6}$$

Normalized eigenvectors are

$$\boldsymbol{\varphi}_j(0,\vartheta) = e^{i\gamma_j(\vartheta)}\frac{\sin v(\vartheta,k)}{\sqrt{a_j(\vartheta,k)}},$$

$$\boldsymbol{\varphi}_j(1,\vartheta) = e^{i\gamma_j(\vartheta)}\exp\left(-i\frac{\vartheta}{2}\right)\frac{i-m_{p,\nu}}{2}\frac{b_j(\vartheta,k)}{\sqrt{a_j(\vartheta,k)}},$$

$$\begin{aligned}a_j(\vartheta,k) &= 1+\sin^2 v(\vartheta,k) \\ &\quad + (-1)^j\cos v(\vartheta,k)\sqrt{1+\sin^2 v(\vartheta,k)},\end{aligned}$$

$$b_j(\vartheta,k) = \cos v(\vartheta,k) + (-1)^j\sqrt{1+\sin^2 v(\vartheta,k)}.$$

The $\gamma_j(\vartheta)$ are arbitrary phases. Discontinuities in the zeros of $a_j(\vartheta,k)$ may be removed by appropriate choices of γ_j. For $k<\pi$ and $-\pi<\vartheta\leq\pi$, one may choose, e.g., $\gamma_j(\vartheta)=\frac{\vartheta}{2}\delta_{j,1}$.

For increasing values of the kicking strength k, eigenphases in Eq. (B6) display thicker and thicker oscillations. An example is shown in Fig. 2(a) for $k=1,3,5$. Nevertheless, contrary to higher values of q, in the case $q=2$, the two eigenphases in Eq. (B6) neither cross nor become closer than a minimal gap, equal to $\pi/2$, for arbitrary high values of k. As a matter of fact, the bandwidth of each eigenvalue, defined as $B_j(k)=|\bar{\omega}(\vartheta_{\max},k)-\bar{\omega}(\vartheta_{\min},k)|$, with $\vartheta_{\max}$ and $\vartheta_{\min}$ absolute maximum and minimum points in $[0,2\pi[$, does not exceed $\pi/2$. For $k<\pi$, $B_j(k)$ is an increasing function of k equal to $B_j(k)=|\bar{\omega}(0,k)-\bar{\omega}(\pi,k)|=|\arccos[\cos(k\cos(\vartheta/2)/\sqrt{2})]-\pi/4|$; for $k>\pi$, $B_j(k)=|\bar{\omega}(\vartheta_1,k)-\bar{\omega}(\pi,k)|=\pi/2$.

Vector and scalar potentials

The vector and scalar potentials can be explicitly computed using analytical expressions of the eigenvectors of resonant fiber (B4). First one computes

$$S_j(\vartheta) = \sum_{l=0}^{1} l|\langle l|\boldsymbol{\varphi}_j(\vartheta)\rangle|^2 = \frac{1}{2}\frac{(b_j)^2}{a_j},$$

$$S_j''(\vartheta) = \sum_{l=0}^{1} l^2|\langle l|\boldsymbol{\varphi}_j(\vartheta)\rangle|^2 = S_j,$$

$$\begin{aligned}S_j'(\vartheta) &= \sum_{l=0}^{1} l\langle\boldsymbol{\varphi}_j(\vartheta)|l\rangle\langle l|\dot{\boldsymbol{\varphi}}_j(\vartheta)\rangle \\ &= \frac{1}{2a_j}\left[b_j\dot{b}_j - \frac{1}{2a_j}\dot{a}_j b_j^2 + i b_j^2\left(\dot{\gamma}_j - \frac{1}{2}\right)\right],\end{aligned}$$

$$i\langle\boldsymbol{\varphi}_j(\vartheta)|\dot{\boldsymbol{\varphi}}_j(\vartheta)\rangle = -\dot{\gamma}_j(\vartheta) + \frac{1}{4}\frac{b_j^2}{a_j},$$

$$\langle \dot{\boldsymbol{\varphi}}_j(\vartheta)|\dot{\boldsymbol{\varphi}}_j(\vartheta)\rangle = \frac{1}{a_j}\left(\dot{v}^2\cos^2 v + \frac{1}{2}\dot{b}_j^2 + \frac{1}{8}b_j^2 - \frac{1}{4}\frac{\dot{a}_j^2}{a_j}\right) + \dot{\gamma}_j\left(\dot{\gamma}_j - \frac{b_j^2}{2a_j}\right),$$

and then, with the particular choice $\gamma_j(\vartheta)=\frac{\vartheta}{2}\delta_{j,1}$, valid for $k<\pi$, the vector and scalar potentials are given by

$$\mathcal{A}_j(\vartheta) \equiv \alpha_j = -\frac{1}{2}\delta_{j,1},$$

$$\mathcal{B}_j(\vartheta) = \frac{4}{a_j}\left(\dot{v}^2\cos^2 v + \frac{1}{2}\dot{b}_j^2 - \frac{1}{4}\frac{\dot{a}_j^2}{a_j}\right) = \frac{2\dot{v}^2}{(1+\sin^2 v)^2}, \tag{B8}$$

with $v \equiv v(\vartheta,k)=k\cos(\vartheta/2)$.

For $q=1$ the resonant fiber is a matrix with a single element $\exp[-iv(\vartheta,k)]$ with eigenfunction $\varphi_0(\vartheta)=\exp(in\vartheta)/\sqrt{2\pi}$ $(n\in\mathbb{Z})$; $S_0=S_0'=S_0''=0$ and therefore it yields, from Eqs. (22) and (23), $\mathcal{A}_0(\vartheta)\equiv\alpha_0=-n$ with $n\in\mathbb{Z}$ and $\mathcal{B}_0(\vartheta)=0$.

[1] G. Casati, B. V. Chirikov, F. M. Izrailev, and J. Ford, *Stochastic Behavior of a Quantum Pendulum Under a Periodic Perturbations*, Lecture Notes in Physics Vol. 93, edited by G. Casati and J. Ford (Springer, Berlin, 1979).

[2] F. M. Izrailev, Phys. Rep. **196**, 299 (1990); S. Fishman, in *Quantum Chaos*, Proceedings of the International School of Physics "Enrico Fermi," Course CXIX, Varenna, edited by G. Casati, I. Guarneri, and U. Smilansky (North-Holland, Amsterdam, 1993).

[3] R. Lima and D. Shepelyansky, Phys. Rev. Lett. **67**, 1377 (1991).

[4] T. Geisel, R. Ketzmerick, and G. Petschel, Phys. Rev. Lett. **67**, 3635 (1991).

[5] R. Artuso, F. Borgonovi, I. Guarneri, L. Rebuzzini, and G. Casati, Phys. Rev. Lett. **69**, 3302 (1992).

[6] I. Guarneri and F. Borgonovi, J. Phys. A **26**, 119 (1993).

[7] A. Backer, R. Ketzmerick, and A. G. Monastra, Phys. Rev. Lett. **94**, 054102 (2005).

[8] A. Backer, R. Ketzmerick, S. Lock, and L. Schilling, Phys. Rev. Lett. **100**, 104101 (2008).

[9] M. Sheinman, S. Fishman, I. Guarneri, and L. Rebuzzini, Phys. Rev. A **73**, 052110 (2006).

[10] J. Feist, A. Backer, R. Ketzmerick, S. Rotter, B. Huckestein, and J. Burgdorfer, Phys. Rev. Lett. **97**, 116804 (2006).

[11] A. Ossipov, T. Kottos, and T. Geisel, Europhys. Lett. **62**, 719 (2003).

[12] F. Borgonovi, I. Guarneri, and L. Rebuzzini, Phys. Rev. Lett. **72**, 1463 (1994).

[13] F. B. Dunning, J. C. Lancaster, C. O. Reinhold, S. Yoshida, and J. Burgdörfer, Adv. At., Mol., Opt. Phys. **52**, 49 (2005).

[14] G. G. Carlo, G. Benenti, and D. L. Shepelyansky, Phys. Rev. Lett. **95**, 164101 (2005).

[15] H. Schanz, M. F. Otto, R. Ketzmerick, and T. Dittrich, Phys. Rev. Lett. **87**, 070601 (2001).

[16] C. E. Creffield, G. Hur, and T. S. Monteiro, Phys. Rev. Lett. **96**, 024103 (2006).

[17] I. Dana, V. Ramareddy, I. Talukdar, and G. S. Summy, Phys. Rev. Lett. **100**, 024103 (2008).

[18] F. L. Moore, J. C. Robinson, C. F. Bharucha, B. Sundaram, and M. G. Raizen, Phys. Rev. Lett. **75**, 4598 (1995).

[19] H. Ammann, R. Gray, I. Shvarchuck, and N. Christensen, Phys. Rev. Lett. **80**, 4111 (1998).

[20] P. Szriftgiser, J. Ringot, D. Delande, and J. C. Garreau, Phys. Rev. Lett. **89**, 224101 (2002).

[21] C. Ryu, M. F. Andersen, A. Vaziri, M. B. d'Arcy, J. M. Grossmann, K. Helmerson, and W. D. Phillips, Phys. Rev. Lett. **96**, 160403 (2006).

[22] M. K. Oberthaler, R. M. Godun, M. B. d'Arcy, G. S. Summy, and K. Burnett, Phys. Rev. Lett. **83**, 4447 (1999).

[23] R. M. Godun, M. B. d'Arcy, M. K. Oberthaler, G. S. Summy, and K. Burnett, Phys. Rev. A **62**, 013411 (2000).

[24] S. Schlunk, M. B. d'Arcy, S. A. Gardiner, and G. S. Summy, Phys. Rev. Lett. **90**, 124102 (2003).

[25] M. B. d'Arcy, R. M. Godun, D. Cassettari, and G. S. Summy, Phys. Rev. A **67**, 023605 (2003).

[26] M. V. Berry and E. Bodenschatz, J. Mod. Opt. **46**, 349 (1999).

[27] S. Fishman, I. Guarneri, and L. Rebuzzini, Phys. Rev. Lett. **89**, 084101 (2002).

[28] S. Fishman, I. Guarneri, and L. Rebuzzini, J. Stat. Phys. **110**, 911 (2003).

[29] I. Guarneri, L. Rebuzzini, and S. Fishman, Nonlinearity **19**, 1141 (2006).

[30] R. Hihinashvili, T. Oliker, Y. S. Avizrats, A. Jomin, S. Fishman, and I. Guarneri, Physica D **226**, 1 (2007).

[31] G. Behinaein, V. Ramareddy, P. Ahmadi, and G. S. Summy, Phys. Rev. Lett. **97**, 244101 (2006).

[32] L. Rebuzzini, R. Artuso, S. Fishman, and Italo Guarneri, Phys. Rev. A **76**, 031603(R) (2007).

[33] P. L. Halkyard, M. Saunders, S. A. Gardiner, and K. J. Challis, Phys. Rev. A **78**, 063401 (2008).

[34] G. Lemarie and K. Burnett, e-print arXiv:quant-ph/0602204 [physics.atom-ph].

[35] M. Saunders, P. L. Halkyard, S. A. Gardiner, and K. J. Challis, e-print arXiv:0806.3894.

[36] I. Guarneri and L. Rebuzzini, Phys. Rev. Lett. **100**, 234103 (2008).

[37] G. Summy (private communication).

[38] F. M. Izrailev and D. L. Shepelyanskii, Theor. Math. Phys. **43**, 553 (1980).

[39] R. G. Littlejohn and W. G. Flynn, Phys. Rev. A **44**, 5239 (1991).

[40] R. G. Littlejohn and W. G. Flynn, Phys. Rev. A **45**, 7697 (1992).

[41] G. Casati and I. Guarneri, Commun. Math. Phys. **95**, 121 (1984).

[42] V. V. Sokolov, O. V. Zhirov, D. Alonso, and G. Casati, Phys. Rev. Lett. **84**, 3566 (2000).

[43] V. V. Sokolov, O. V. Zhirov, D. Alonso, and G. Casati, Phys.

Rev. E **61**, 5057 (2000).
[44] J. Farey, Philos. Mag. J. **47**, 385 (1816).
[45] G. H. Hardy and E. M. Wright, *An Introduction to the Theory of Numbers* (Clarendon, Oxford, 1979).
[46] I. Dana and D. L. Dorofeev, Phys. Rev. E **73**, 026206 (2006).
[47] S. J. Chang and K. J. Shi, Phys. Rev. A **34**, 7 (1986).
[48] S. Teufel, *Adiabatic Perturbation Theory in Quantum Dynamics*, Lecture Notes in Mathematics Vol. 1821 (Springer, Berlin, 2003).
[49] I. Dana, E. Eisenberg, and N. Shnerb, Phys. Rev. Lett. **74**, 686 (1995).
[50] M. V. Berry, Proc. R. Soc. London, Ser. A **392**, 45 (1984).
[51] B. Simon, Phys. Rev. Lett. **51**, 2167 (1983).
[52] A. Buchleitner, M. B. d'Arcy, S. Fishman, S. A. Gardiner, I. Guarneri, Z. Y. Ma, L. Rebuzzini, and G. S. Summy, Phys. Rev. Lett. **96**, 164101 (2006).
[53] I. Dana and V. Roitberg, Phys. Rev. E **76**, 015201(R) (2007).